J Neurooncol (2009) 91:337–351
DOI 10.1007/s11060-008-9719-x

CLINICAL STUDY - PATIENT STUDY

Relationship of pre-surgery metabolic and physiological MR imaging parameters to survival for patients with untreated GBM

Forrest W. Crawford · Inas S. Khayal · Colleen McGue · Suja Saraswathy · Andrea Pirzkall · Soonmee Cha · Kathleen R. Lamborn · Susan M. Chang · Mitchel S. Berger · Sarah J. Nelson

Received: 17 March 2008 / Accepted: 13 October 2008 / Published online: 15 November 2008

Abstract Glioblastoma Multiforme (GBM) are heterogeneous lesions, both in terms of their appearance on anatomic images and their response to therapy. The goal of this study was to evaluate the prognostic value of parameters derived from physiological and metabolic images of these lesions. Fifty-six patients with GBM were scanned immediately before surgical resection using conventional anatomical MR imaging and, where possible, perfusion-weighted imaging, diffusion-weighted imaging, and proton MR spectroscopic imaging. The median survival time was 517 days, with 15 patients censored. Absolute anatomic lesion volumes were not associated with survival but patients for whom the combined volume of contrast enhancement and necrosis was a large percentage of the T2 hyperintense lesion had relatively poor survival. Other volumetric parameters linked with less favorable survival were the volume of the region with elevated choline to *N*-acetylaspartate index (CNI) and the volume within the T2 lesion that had apparent diffusion coefficient (ADC) less than 1.5 times that in white matter. Intensity parameters associated with survival were the maximum and the sum of levels of lactate and of lipid within the CNI lesion, as well as the magnitude of the 10th percentile of the normalized ADC within the contrast-enhancing lesion. Patients whose imaging parameters indicating that lesions with a relatively large percentage with breakdown of the blood brain barrier or necrosis, large regions with abnormal metabolism or areas with restricted diffusion have relatively poor survival. These parameters may provide useful information for predicting outcome and for the stratification of patients into high or low risk groups for clinical trials.

Keywords Newly diagnosed glioblastoma multiforme · MRSI · DWI · PWI · Survival

F. W. Crawford · I. S. Khayal · S. Saraswathy · S. J. Nelson (✉)
Department of Radiology, University of California, San Francisco, Box 2532, 1700 4th Street, San Francisco, CA 94143-2532, USA
e-mail: sarah.nelson@radiology.ucsf.edu

I. S. Khayal · C. McGue · S. Cha · S. J. Nelson
UCSF/UCB Joint Graduate Group in Bioengineering, University of California, San Francisco, CA, USA

A. Pirzkall
Department of Radiation Oncology, University of California, San Francisco, CA, USA

S. Cha · K. R. Lamborn · S. M. Chang · M. S. Berger
Department of Neurological Surgery, University of California, San Francisco, CA, USA

Introduction

Even with aggressive resection and the use of state-of-the-art therapies, survival for patients who are diagnosed with Glioblastoma Multiforme (GBM) is relatively short and there is great interest in developing new treatment strategies that are likely to be more effective [1–3]. There is considerable variability for individual patients, with the median survival from the time of diagnosis being from 1 to 2 years [1, 4–6] and a recent analysis of 766 patients reporting that only 2% were alive after 5 years [7]. Given such a bleak prognosis and the need to determine which patients might benefit from new therapies, it is important to identify non-invasive biomarkers that can be used to characterize individual lesions and to predict outcome [1, 6, 8, 9].

Although contrast-enhancing regions give valuable information regarding the location of different tumors [9, 10], there is considerable evidence to demonstrate that

metabolic markers of malignancy are present outside of the contrast enhancing region [9–11]. The region of T2-hyperintensity is larger than the enhancing volume but cannot distinguish between peritumoral edema and infiltrative tumor [1, 9, 12]. Perfusion-weighted imaging (PWI), diffusion weighted imaging (DWI) and MR spectroscopic imaging (MRSI) have been proposed as methods that may offer more detailed information regarding tumor burden and malignant behavior. PWI measures hemodynamic properties such as tissue blood volume, vessel leakiness and permeability [13–15]. DWI gives information about the apparent diffusion coefficient (ADC) of water which has been reported as providing an early predictor of response to radiation [16–19]. Proton MR spectroscopic imaging (MRSI) gives information regarding the levels of cellular metabolites that may be relevant in evaluating treatment response and clinical outcome [1, 20–22].

Although several factors such as age, Karnofsky Performance Scale (KPS) score, midline shift, and tumor location have been shown to predict survival for large populations of patients with GBM [6, 23, 24]; the importance of the extent of resection and the impact of using these factors to direct the choice of therapy remain controversial [3, 5, 25–27]. If non-invasive imaging parameters are able to predict survival, they could be used to stratify patients into risk groups for future clinical trials of new therapies. More accurate assessment of the baseline risk at the time of diagnosis may thus provide improved treatment selection for individual patients and ultimately enhance their survival. The goal of this study was to characterize patients with untreated GBM prior to surgery using anatomic perfusion, diffusion and spectroscopic markers and to evaluate the potential of these imaging parameters in predicting survival.

Methods

Patient population

Between October 2001 and January 2006, 56 treatment-naïve adults (39 men, 17 women, median age 56, mean age 56 ± 12.8 years) who were subsequently diagnosed as having supratentorial GBM received an MR imaging examination 1 day prior to image-guided surgery. Standard anatomic images were acquired as needed for their clinical care. Whenever possible within the time limitations imposed by this pre-surgery examination, patients also received PWI, DWI and MRSI. Histological diagnosis of GBM was made from tissue obtained at the time of surgical resection. Patients were treated with conformal fractionated radiation therapy administering 60 Gy in standard fractionation) and concurrent and adjuvant chemotherapy, with the majority of them receiving temozolomide (at least 39/56 patients).

MR examination

Patients were imaged using a Signa Echospeed 1.5T scanner (General Electric Healthcare, Milwaukee, WI, USA) using a standard quadrature head coil. The standard pre-surgery imaging protocol for gliomas in our institution includes a T1-weighted three-plane scout (TR/TE = 400/12 ms); pre- and post-contrast T1-weighted 3D spoiled gradient echo (SPGR − TR/TE = 32/8 ms, 40 flip, 180 × 240 × 186 mm FOV, with 192 × 256 × 124 matrix); T2-weighted fluid attenuated inversion recovery (FLAIR − TR/TE/TI = 10,000/143/2,200 ms, 220 × 220 × 160 mm FOV, with 256 × 256 × 32 matrix); T2-weighted fast spin echo (FSE − TR/TE = 3,000/105 ms, 260 × 260 × 180 mm FOV, with 256 × 256 × 120 matrix).

Anatomical images were rigidly aligned to the post-Gd SPGR images using software developed in our group [28]. Tumor region-of-interest segmentation was performed using an in-house semi-automated segmentation software package [29]. The contrast-enhancing (CEL) and necrotic (NEC) regions were contoured on the post-Gd SPGR images. The T2-hyperintense region (T2ALL) was contoured on FSE or FLAIR images. The non-enhancing lesion (NEL) was defined as the T2 lesion minus the contrast-enhancing lesion and necrotic regions. Normal-appearing white matter (NAWM) regions were automatically segmented using the FSL software package [30].

Perfusion-weighted imaging

PWI data were acquired for 49 of the 56 patients. A bolus of 0.1 mmol/kg body weight Gd-DTPA was injected into the antecubital vein at a rate of 5 ml/s. Dynamic susceptibility contrast echoplanar gradient echo images were acquired before, during, and after the passage of the contrast agent. Acquisition parameters were (TR/TE = 1,700/100 ms, matrix = 256 × 256 × 7–9,
FOV = 400 × 400 × 54 mm^3, with a total of 60 time points. The resulting data were processed to yield measures of cerebral blood volume (CBV), and non-parametric estimates of percent ΔR2* recovery (%REC), and ΔR2* peak heights (PH) using in-house software [15, 31–33]. Maps of these parameters were rigidly aligned to the post-contrast T1-weighted images using the VTK software package and then re-sampled to the same spatial resolution.

Diffusion weighted imaging

DWI data were available for 47 of the 56 patients. Two datasets were eliminated due to severe ghosting artifacts, leaving results from a total of 45 patients being considered

for the quantitative analysis. Acquisition parameters were TR/TE = 10,000/100 ms, matrix 128 × 128, FOV = 360 × 360 mm^2 with 38–36 slices and 3–5 mm slice thickness, b value 1,000 s/mm^2, gradient strength = 0.04 T/m, gradient duration = 21 ms, and gradient separation = 27 ms. The diffusion-weighted images were processed to yield apparent diffusion coefficient (ADC) maps using in-house software. The maps were rigidly aligned to the post-contrast T1-weighted images using the VTK software package and then re-sampled to the same spatial resolution [34].

1H MRSI data

Three-dimensional MRSI data were acquired for 50 of the 56 patients. Datasets from two patients had limited coverage of normal appearing white matter so that results from a total of 48 patients were considered for the quantitative analysis. The data were acquired using 3D PRESS volume selection [35] and VSS outer volume suppression bands [36] that were developed in our laboratory. The selected volume was prescribed on the post-contrast T1-weighted image to cover as much of the lesion as possible and to include normal-appearing contralateral tissue. The 3D data were phase-encoded with a 12 × 12 × 8 matrix and fields of view 120 × 120 × 80 mm (TR/TE = 1,000/144 ms). Of the 48 patients considered, 42 of them had lactate-edited spectroscopy and could therefore provide separate estimates of the contributions from lactate and lipid [37]. The spectroscopic data were processed using in-house software that has been described previously [11, 38, 39]. Parameters that are estimated include peak locations, heights, areas, and linewidths for each voxel. For the lactate-edited data, summed acquisitions gave spectra with choline, creatine, NAA and lipid, while the subtracted data gave lactate alone [22, 37].

The choline-to-NAA index (CNI) was estimated as described previously based upon the differences in relative peak heights between tumor and normal tissue [40]. The relationship between metabolite levels and anatomic regions were examined by resampling masks of the regions of interest to match the resolution of the spectral data. Voxels that were predominantly in NAWM, the contrast-enhancing lesion, the necrosis or the non-enhancing lesion, as well voxels that had CNI values greater than 2 or 3 were used to calculate the statistics for the analysis. The registration error for the MRSI data was assumed to be negligible because they were acquired immediately following the post-contrast SPGR images.

Analysis of MR parameters

The anatomic regions of interest were the contrast-enhancing lesion (CEL), the non-enhancing lesion (NEL), necrosis (NEC) and the entire T2 lesion (T2ALL). Lesion volumes and the intensity variations of individual MR parameters were recorded. In cases where the acquisition window for the PWI, DWI and MRSI data was smaller than the spatial extent of one of the anatomical regions, the analysis was limited to the region that overlapped with it. To facilitate comparison of parameter values between patients, the values of ADC, rCBV, PH, choline, creatine and NAA were normalized to their median values within NAWM. Lactate and lipid maps were normalized to the median value of NAA within NAWM. The values of the %REC and CNI were not normalized. Measures of the spatial extent of regions with abnormal PWI and DWI parameters were determined by considering the volume within the T2 lesion that had nCBV greater than 2 or 3 and with nADC less than 1.5. Measures of the spatial extent of the metabolic lesions were obtained by considering the number of voxels with CNI values greater than 2 and the number with CNI greater than 3.

Kaplan–Meier survival curves were computed using standard techniques. The Cox proportional hazards model was used to evaluate the influence of each of the parameters on survival. The Cox model is a semi-parametric survival analysis tool that assumes a fixed baseline hazard for the population and computes regression coefficients for a set of predictor variables. All proportional hazards analyses were controlled for patient age since this as previously been reported as influencing survival [6, 23, 24]. Evaluation of the significance of differences between the values of MR parameters in the various anatomic regions was made using the Wilcoxon rank sum test. Where appropriate, the relationships between variables were investigated using the Spearman rank correlation coefficient.

Results

Survival time was calculated as the number of days between the pre-surgery MR examination and the date of death or last clinical visit in which the patient was known to be alive. The Kaplan–Meier survival curve indicated that the median survival was 517 days (mean 654 days, standard deviation 66 days), with 11 of the 56 patients being censored. Figure 1 shows this survival curve. Note that of the 11 patients that were censored, all were studied for at least 365 days, eight for at least 540 days and the remaining five longer than 730 days. The 95% confidence intervals for the median survival were 374 and 603 days.

Characteristics of anatomic lesions

Fifty-five patients exhibited contrast enhancement and 47 had regions of necrosis as defined by regions of

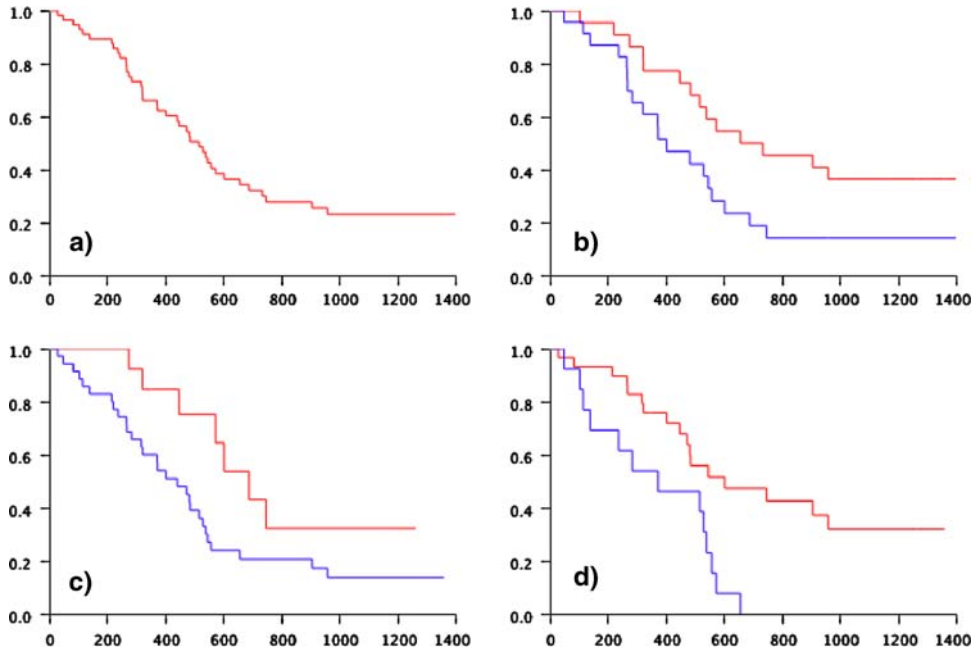

Fig. 1 Kaplan Meier survival curves for 56 patients who were studied with MR prior to surgery and who had a diagnosis of GBM. The overall median survival (**a**) was 517 days, median age 56 years with a range of 26–83. Survival curves (**b**) are for populations split based upon the volume of ADC > 1.5 in the T2 lesion (median survival of 735 days for patients with volumes <31.6 cc, 403 days with volume > 31.6 cc), (**c**) are split based upon the number of voxels with CNI > 2 (median survival of 689 days for smaller volumes and 442 days for larger volumes) and (**d**) are split based upon the value of the sum of lipid peaks in the region with CNI > 2 region (median survival 374 days for large values and 603 days for smaller values)

hypointensity on the T1-weighted SPGR images. The volumes, standard deviations, and ranges of the anatomic lesions were highly variable with the median volume of the contrast-enhancing lesion being 15.3 cc, of necrosis being 2.7 cc and of the entire T2 lesion being 60.8 cc (see Table 1). The median percentage of the T2 lesion that was contrast enhancing was 24%, the median percentage that was necrotic was 5% and the median percentage that was non-enhancing was 68%. The volumes of contrast enhancement and necrosis were highly correlated based upon the Spearman rank test ($P < 0.0001$, $n = 47$) but neither of these showed significant correlation with the volume of the non-enhancing lesion ($P = 0.146$, $n = 55$ and $P = 0.219$, $n = 47$, respectively).

The proportional hazards analysis indicated that the only anatomic variable with a relationship to survival having a P value less than 0.05 was the sum of the enhancing and necrotic volumes as a percentage of the T2 lesion (%CEL + NEC) which had median value $33 \pm 23\%$. Figure 2 shows examples of patients who each had lesions with large T2 lesion volumes. The patient on the left (survival 116 days) had a thin rim of enhancement and a large volume of necrosis, while the patient on the right (survival 267 days) had a relatively large volume of contrast enhancement. When the patient population was split based upon whether the %CEL + NEC was greater than the 75th percentile of the value for the population as a whole, the difference between survival curves was

Table 1 Median volumes and standard deviations of the volumes of anatomic lesions

	CEL ($n = 55$)	NEC ($n = 47$)	CEL + NEC ($n = 55$)	NEL ($n = 56$)	T2ALL ($n = 56$)
Median (cc)	15.3	2.7	22.7	43.3	60.8
SD	16.6	8.1	20.8	33.5	40.3
	$P = 0.188$	$P = 0.386$	$P = 0.212$	$P = 0.433$	$P = 0.457$
Median %T2ALL	24	5	33	68	–
SD	17	12	23	23	
	$P = 0.074$	$P = 0.066$	$P = 0.026$*	–	

The percentage of the T2 hyperintense region that was contrast enhancing and necrotic (as well as the complementary percentage that was non-enhancing) had P values from the Proportional Hazards analysis which suggesting that it was associated with survival. The * defines parameters for which the proportional hazards analysis gave a P value of less then 0.05

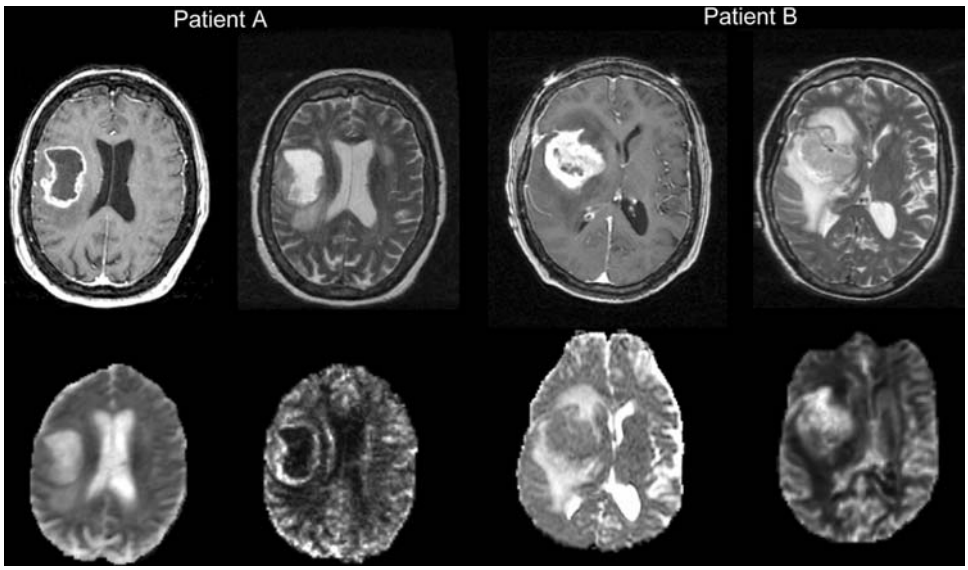

Fig. 2 Post-contrast T1-weighted, T2-weighted, nCBV and ADC images from patients with GBM who had large %CEL + NEC and had relatively poor outcome. Patient A had a survival of 116 days, age = 53, %CEL = 17, %NEC = 16, T2all volume = 67 cc and nADC10%(CEL) = 1.13. Patient B had a survival of 267 days, age = 71, %CEL = 24, %NEC = 1, T2all volume = 142 cc and nADC10%(CEL) = 1.00

significant based upon a Wilcoxon test ($P = 0.036$) but not the log rank test ($P = 0.088$). The median survival for the population with larger percentage volumes was 322 days, compared with a median of 531 days for the population with smaller percentage volumes.

PWI parameters

Table 2 shows the median and 90th percentile values of the perfusion-weighted imaging parameters nCBV, nPH and %REC in each of the segmented anatomic regions. The nCBV values were highest in the contrast-enhancing lesion and were either equal to or higher than NAWM values in the non-enhancing and necrotic region. From the Wilcoxon rank sum test only the CBV values in the contrast enhancement consistently showed significant differences from NAWM. The values of the nPH were highly correlated with the nCBV intensities and showed similar trends within all of the regions studied. The median REC was 88% in NAWM, 83% in the contrast-enhancing lesion and 88% in the non-enhancing lesion. None of the regional intensities of these parameters showed a significant relationship with survival.

Figure 2 includes examples of nCBV maps from regions of enhancement and necrosis. Note that the regions with elevated nCBV are within the contrast enhancement and there is relatively low intensity within necrosis. Figure 3 provides arrays of concentration-time curves from three different lesions. The one on the left is the same patient as in Fig. 2 and shows that there are variations in both peak height (PH) and recovery (%REC) within the large contrast enhancement. Note that the curves in regions corresponding to necrosis are essentially flat, showing very little change in signal intensity. Although the patients in the middle and on the right panel of Fig. 3 have regions with elevated peak height in the contrast enhancement, they have relatively long survival (658 days and >1,361 days,

Table 2 Perfusion weighted imaging parameters: normalized CBV (nCBV), normalized peak height (PH) and recovery (%REC) parameters for normal appearing white matter, contrast-enhancing lesion, necrotic lesion and non-enhancing lesion

	NAWM ($n = 49$)	CEL ($n = 48$)	NEC ($n = 41$)	NEL ($n = 49$)
nCBV Median	1.00	1.89	0.93	1.09
SD	–	0.84	0.94	0.42
nCBV 90%	2.03	3.69	2.17	2.58
SD	0.26	1.28	1.48	0.71
nPH Median	1.00	1.74	0.87	0.96
SD	–	0.91	1.02	0.42
nPH 90%	1.99	3.37	1.89	2.28
SD	0.25	1.49	1.68	0.80
%REC Median	88	83	89	88
SD	4	6	9	6
%REC 10%	81	70	74	767
SD	4	10	12	7
Volumes (cc) within T2ALL	nCBV > 3	%nCBV > 3	nCBV > 2	%nCBV > 2
Median	3.4	9.3	8.9	25.7
SD	5.4	10.7	8.7	14.3

The lower values represent the volumes of sub-regions with high nCBV values that were in the region of the T2 hyperintensity that was covered by the PWI volume (median 40.8 ± 20.9 cc). There were no significant correlations to survival for any of these perfusion parameters

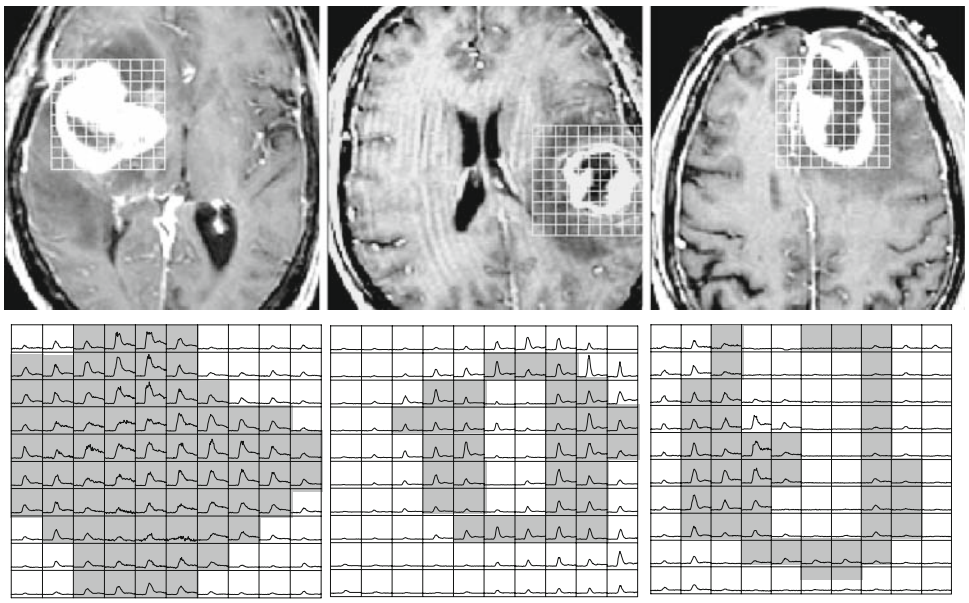

Fig. 3 T1-weighted post-contrast images from three patients with GBM and arrays of concentration time curves showing the spatial distribution and magnitude of peak height and recovery parameters. Patient B on the left had survival of 267 days and age = 49 with the 10th percentile of %REC = 57 and 90th percentile of nCBV = 6.0. Patient C in the center had survival of 648 days and age = 49 with the 10th percentile of %REC = 72 and 90th percentile of nCBV = 6.4. Patient D on the right had a survival >1,361 days and age of 54 with the 10th percentile of %REC = 70 and 90th percentile of nCBV = 3.7

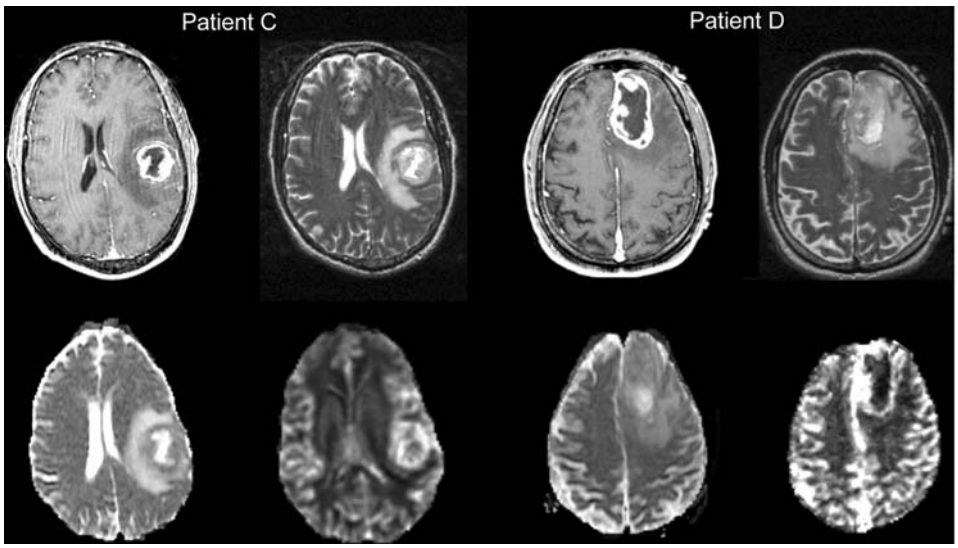

Fig. 4 Post-contrast T1-weighted, T2-weighted, nCBV and ADC images from patients C and D from Fig. 3 who had relatively long survival. Both patients had elevated nCBV but the ADC values within the CEL volume was larger than for patients A and B from Fig. 1. Patient C, who was assessed as receiving a gross total resection, had a survival of 658 days, age = 49, %CEL = 14, %NEC = 8, T2ALL volume = 104 cc and nADC10%(CEL) = 1.30. Patient D had a survival >1,361 days, age = 54, %CEL = 27, %NEC = 16, T2ALL volume = 92 cc and nADC10%(CEL) = 1.24

respectively). Figure 4 shows the anatomic images and nCBV maps from these two patients, which underline the close correspondence between the contrast enhancement and the region with elevated blood volume.

The maps of nCBV in Figs. 2 and 4 demonstrate that the signal intensity in gray matter may be similar to that in contrast enhancement, which means that defining the spatial extent of the region with abnormal vasculature requires the anatomic images to provide context. In our analysis, cut-off values of two or three times that in NAWM were used to define the fraction of the T2 lesion that had abnormal nCBV. The median volume with nCBV > 3 was 3.4 cc, which corresponded to 8.5% of the median volume of the T2 lesion, while the median volume with nCBV > 2 was 8.9 cc or 26%. Note that both of these values were considerably smaller than the volumes of the contrast enhancement, which had a median value of 15.3 cc. The percentage of the T2 lesion covered by the perfusion acquisition was 65%, and the median percentage of contrast enhancement that was covered was 71%.

DWI parameters

The median ADC parameters in the various anatomic regions are shown in Table 3. The highest value was found in necrosis (1,509), followed by the non-enhancing lesion (1,222), contrast enhancement (1,156) and NAWM (801). Wilcoxon rank sum tests performed on these values indicated that each pair was significantly different from the others. The ADC maps in Figs. 2 and 4 show that there were large differences in ADC values between contrast enhancement and necrosis, with the ADC being highly variable in the non-enhancing lesion, presumably due to the existence of sub-regions of edema and infiltrative tumor. Comparison of the values of the 10th percentile of the ADC and nADC in different regions indicated that there were sub-regions within the contrast-enhancing lesion, necrosis and the non-enhancing lesion that had similar ADC values.

The results of the proportional hazards analysis of ADC intensities within the contrast enhancement and necrosis showed that low 10th percentile values were associated with poor survival. This observation was further supported by the observation that patients with large v(nADC < 1.5) (volume within the T2 lesion having nADC less than 1.5) had worse survival. Note that the median v(nADC < 1.5) was twice the size of the median volume of contrast enhancement (31.6 cc compared with 15.3 cc). When the patient populations were split based upon whether v(nADC < 1.5) was greater or less than its median value, the survival curves were significantly different based upon both the log-rank test ($P = 0.04$) and Wilcoxon test ($P = 0.03$). The median survival for the population with larger v(nADC < 1.5) was 403 days (mean 438 days, standard deviation 47 days), compared with a median of 735 days (mean 840 days, standard deviation 107 days) for the population with smaller volumes (see Fig. 1).

Table 3 Median and 10th percentile intensity values for ADC and normalized ADC within different anatomic regions, followed by the volumes within the T2ALL that had the normalized ADC or nADC values indicated

	NAWM ($n = 45$)	CEL ($n = 44$)	NEC ($n = 40$)	NEL ($n = 45$)
ADC Median	801	1,156	1,509	1,222
SD	50	183	467	200
		$P = 0.080$	$P = 0.286$	$P = 0.350$
ADC 10%	664	847	998	912
SD	35	184	333	134
		$P = 0.026$*	$P = 0.033$*	$P = 0.261$
nADC Median	1.00	1.44	1.74	1.47
SD		0.23	0.58	0.27
		$P = 0.062$	$P = 0.190$	$P = 0.315$
nADC 10%	0.83	1.11	1.22	1.06
SD	0.04	0.24	0.41	0.19
		$P = 0.028$*	$P = 0.017$*	$P = 0.248$

Volumes in T2ALL (cc)	nADC < 1.5	nADC < 1.25
Median	31.6	17.0
SD	17.2	15.7
	$P = 0.047$*	$P = 0.050$

The P values represent the results of Proportional Hazards analysis that included age as a covariate and the values with a * indicate ($P < 0.05$)

Levels of choline, creatine and NAA

Table 4 gives metabolite levels and corresponding metabolic indices within the portion of the anatomic lesions that overlapped with the PRESS volume. The median NAA, creatine and choline were lowest in necrosis (0.13, 0.09, and 0.52), presumably reflecting that it contained the lowest number of viable cells. The median levels of NAA and creatine were higher in the non-enhancing lesion (0.39 and 0.90) than in the contrast enhancement (0.22 and 0.58). The median choline was similar in these two regions (1.17 vs. 1.13) but the maximum choline was marginally higher in the non-enhancing lesion. The variations in levels of these metabolites meant that the median CNI was greater for all tumor regions than in NAWM. While the median value was highest in the contrast-enhancing lesion, the

Table 4 Levels of metabolites in the anatomic and CNI > 2 regions and numbers of voxels within the region of T2 hyperintensity that were covered by the MRSI data acquisition

	NAWM ($n = 48$)	CEL ($n = 46$)	NEC ($n = 42$)	NEL ($n = 48$)	CNI2 ($n = 48$)
NAA median	1.00	0.22	0.13	0.39	0.43
SD	–	0.14	0.15	0.19	0.24
Cre median	1.00	0.58	0.09	0.90	0.98
SD	–	0.52	0.45	0.53	0.40
Cho median	1.00	1.17	0.52	1.13	1.46
SD		1.21	0.98	0.78	0.58
Cho max	1.21	1.63	0.83	1.77	2.35
SD	0.26	1.83	1.00	2.26	2.16
CNI median	−0.03	4.17	1.28	1.90	3.32
SD	0.78	3.74	3.39	3.99	1.26
CNI max	0.29	5.69	2.48	5.72	6.63
SD	1.01	5.16	3.26	6.15	5.86
CNI sum	−0.7	3.8	13.7	38.3	115.3
SD	2.7	7.2	41.2	97.6	148.8

Number of voxels	CNI > 2	CNI > 3	Within T2ALL
Median	34.0	17.5	53.9
SD	34.6	18.8	25.9

maximum was similar in the non-enhancing lesion and the contrast-enhancing lesion. This implies that there were subregions of the non-enhancing lesion with metabolic characteristics that were similar or more abnormal than those within the contrast-enhancing lesion. None of these intensity values had a statistically significant association with survival.

Figure 5 shows examples of spectra from lesions that have voxels with CNI > 2 extending outside the contrast-enhancing lesion. Voxels highlighted in blue have CNI > 2 and low lipid, while voxels highlighted in red have CNI > 2 and elevated lipid. Although the two patients on the left have relatively large regions with elevated choline and reduced NAA, none of the MRSI voxels had high lipid. Their survival was 906 and 907 days. For the patient on the right, who had both diffuse enhancement and necrosis, there were a substantial number of voxels with both high CNI and elevated lipid peaks. This patient had a relatively short survival of 109 days.

The median number of voxels in the T2 lesion that were covered by the PRESS region and had CNI > 2 was 34, while the number of voxels with CNI > 3 was 17.5. The median percentages of the T2 lesion and the contrast-enhancing lesion that were covered by the PRESS selected volume were 54 and 59%, respectively. The Proportional Hazards analysis indicated that the volume of the region with CNI greater than 2, v(CNI > 2), was associated with survival with a P value of 0.034. When the patient population was split based upon the 25th percentile of v(CNI > 2), the survival curves were different based upon both the log-rank test ($P = 0.05$) and Wilcoxon test ($P = 0.03$). The median survival for the population with larger v(CNI > 2) was 442 days (mean 466 days, standard deviation 151 days) and compared with a median survival of 689 days (mean 610 days, standard deviation 51 days) for the population with smaller v(CNI > 2).

Levels of lactate and lipid

Table 5 shows the median, maximum and sum of values for lactate and lipid within the intersection of the PRESS volume and anatomic regions. In all cases the most extreme values are in necrosis or the contrast-enhancing lesion. Of interest is that the maximum and sum of lipid intensities within the region having CNI > 2 were associated with survival ($P = 0.035$ and $P = 0.003$, respectively). The proportional hazards analysis of the maximum and sum of lactate intensities in the region with CNI > 2 gave P values of 0.037 and 0.038, respectively. Figures 6, 7 and 8 give examples of differences in the spatial patterns of metabolites for three of the patients whose MR examinations included the acquisition of lactate-edited data. The voxels highlighted in blue and red have similar properties to the ones defined above, while the voxels in yellow have elevated lipid but low levels of choline, creatine and NAA and the voxels in green have elevated lactate. The patient in Fig. 6 who had a small number of abnormal voxels was still alive after 1,161 days, while the patient in Fig. 7 had a

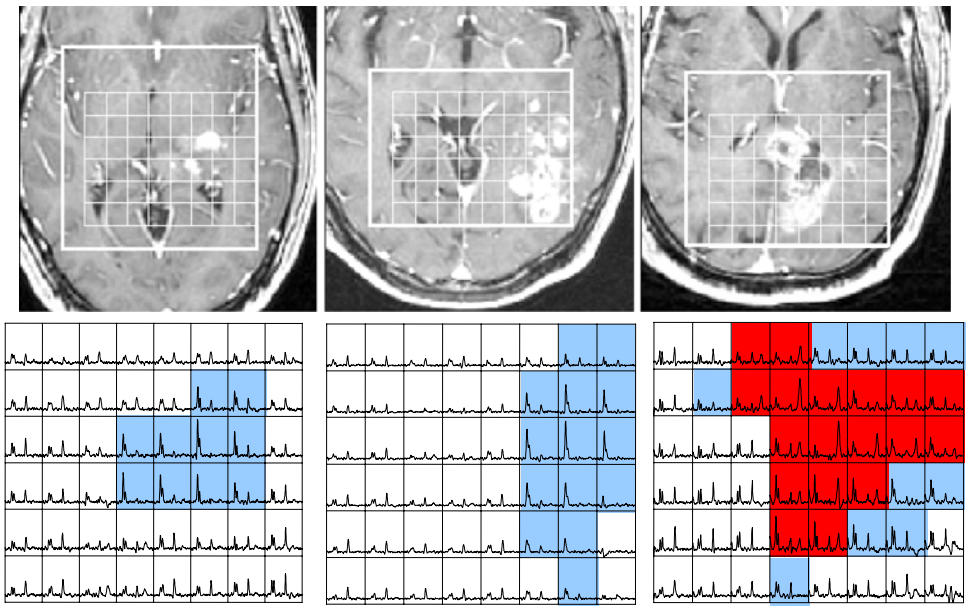

Fig. 5 MR images and spectra from patients with GBM who had large number of voxels with elevated CNI outside the CEL. Reading from left to right the peaks observed are choline, creatine, NAA, and lipid. Voxels in blue have CNI > 2, voxels in red have both CNI > 2 and elevated lipid. Patient E had survival of 906 days, age = 56, number of CNI voxels > 2 = 49 and number with elevated lipid = 3. Patient F had survival of 907 days, age = 582, number of CNI voxels > 2 = 53 and number with elevated lipid = 5. Patient G had survival of 104 days, age = 63, number of CNI voxels > 2 = 58 and number with elevated lipid = 43

Table 5 Levels of lactate and lipid in the anatomic and CNI > 2 regions normalized by the level of NAA in NAWM

	NAWM ($n = 42$)	CEL ($n = 40$)	NEC ($n = 35$)	NEL ($n = 42$)	CNI2 ($n = 42$)
LAC median	0.06	0.25	0.30	0.15	0.17
SD	0.08	0.20	0.35	0.12	0.08
		$P = 0.230$	$P = 0.254$	$P = 0.068$	$P = 0.250$
LAC max	0.11	0.35	0.45	0.32	0.43
SD	0.08	0.25	0.37	0.31	0.28
		$P = 0.261$	$P = 0.213$	$P = 0.153$	$P = 0.037$*
LAC sum	0.12	0.47	0.82	2.60	4.45
SD	0.54	3.56	7.53	4.50	5.89
		$P = 0.208$	$P = 0.592$	$P = 0.219$	$P = 0.038$*
LIP median	0.02	0.34	0.46	0.08	0.14
SD	0.22	0.56	0.78	0.30	0.16
		$P = 0.198$	$P = 0.378$	$P = 0.025$*	$P = 0.370$
LIP max	0.13	0.83	0.56	0.31	0.54
SD	0.24	0.64	0.98	0.77	0.78
		$P = 0.170$	$P = 0.229$	$P = 0.236$	$P = 0.035$*
LIP sum	0.06	0.55	1.85	1.99	4.31
SD	0.49	5.26	2.61	3.24	7.44
		$P = 0.194$	$P = 0.373$	$P = 0.146$	$P = 0.003$*

The * defines parameters for which the proportional hazards analysis gave a P value of less then 0.05

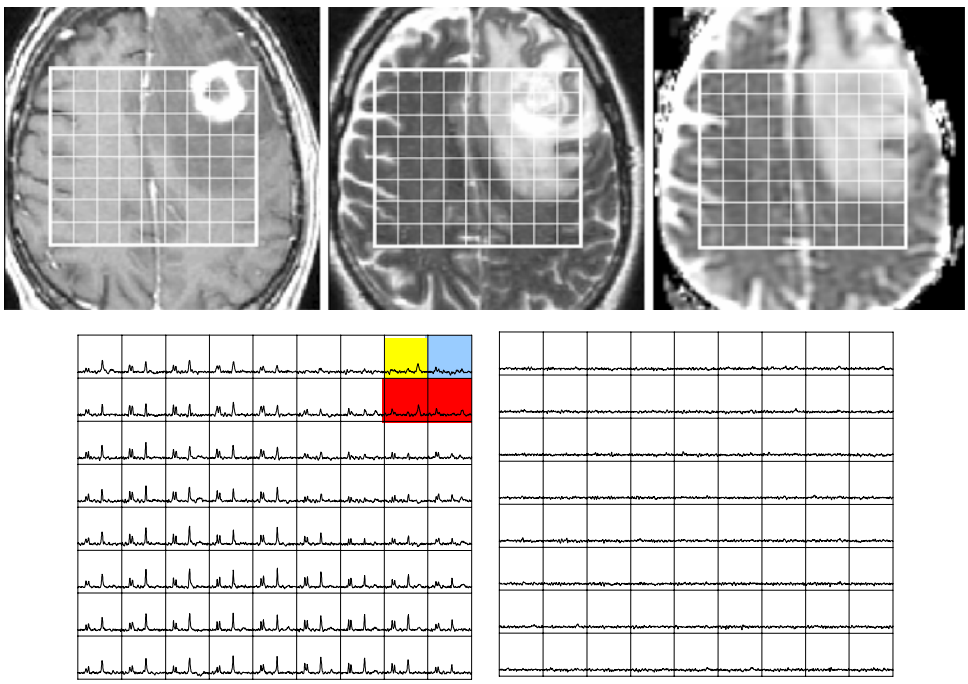

Fig. 6 MR images and spectra from a patient (E) who had a GBM with a large T2 volume but small enhancing lesion. Voxels in blue had CNI > 2, voxels in red had CNI > 2 with elevated lipid, voxels in yellow had elevated lipid but CNI value less than 2. For this patient age = 65, survival > 1,161 days, number of voxels with CNI > 2 = 7, number of voxels with elevated lip = 13, none with elevated lactate, sum of lipid intensities in CNI > 2 = 2.48, 10th percentile of nADC in the CEL = 1.17, %CEL + NEC = 15, T2ALL volume = 139 cc

survival of 558 days and the patient in Fig. 8 a survival of 104 days.

Analysis of survival for combinations of variables

Although the analysis of single variables identified MR parameters that are relevant in predicting outcome for patients with GBM some of the P values obtained were relatively modest. To determine whether combinations of variables might improve the ability to assess prognosis, six representative variables were selected and evaluated in a pair-wise fashion. Volumetric measures were the %(CEL + NEC), v(ADC < 1.5) and v(CNI > 2). Three intensity parameters were chosen; the 10th percentile of nADC in the contrast-enhancing lesion (nADC10%(CEL)), the sum of lactate peaks in the region with CNI greater than

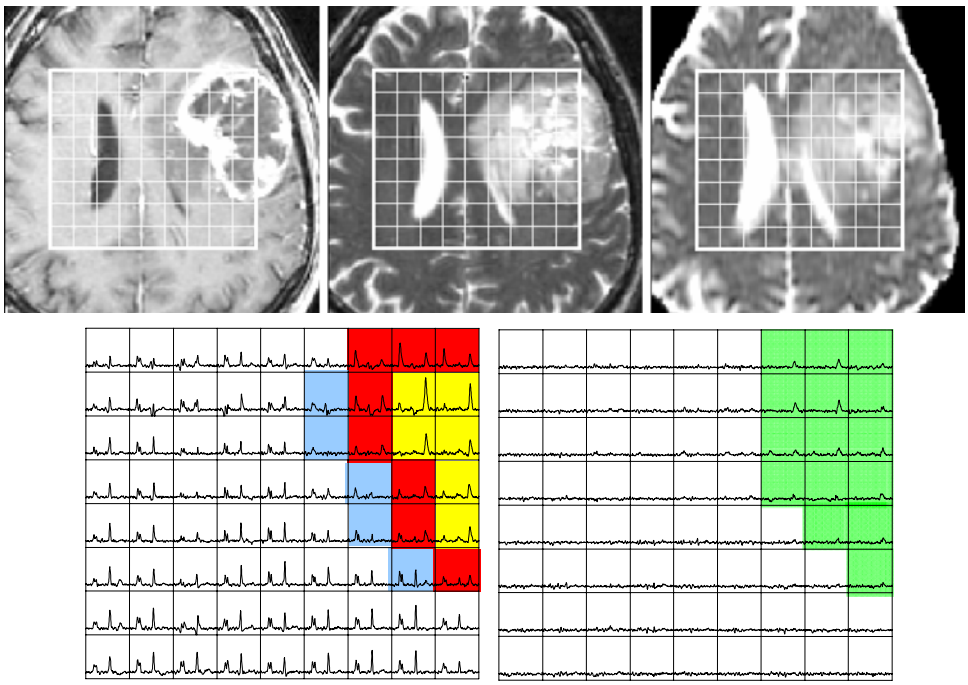

Fig. 7 MR images and spectra from a patient (F) who had a GBM with a large T2 volume, relatively large enhancing lesion but a large number of voxels having abnormal CNI and elevated lipid and lactate. Voxels in blue had CNI > 2, voxels in red had CNI > 2 with elevated lipid, voxels in yellow had elevated lipid but CNI value less than 2. For this patient age = 62, survival 558 days, number of voxels with CNI > 2 = 42, number of voxels with elevated lip = 42, sum of lipid intensities in CNI > 2 = 17.4, 10th percentile of nADC in the CEL = 1.13, %CEL + NEC = 27, T2ALL volume = 134 cc

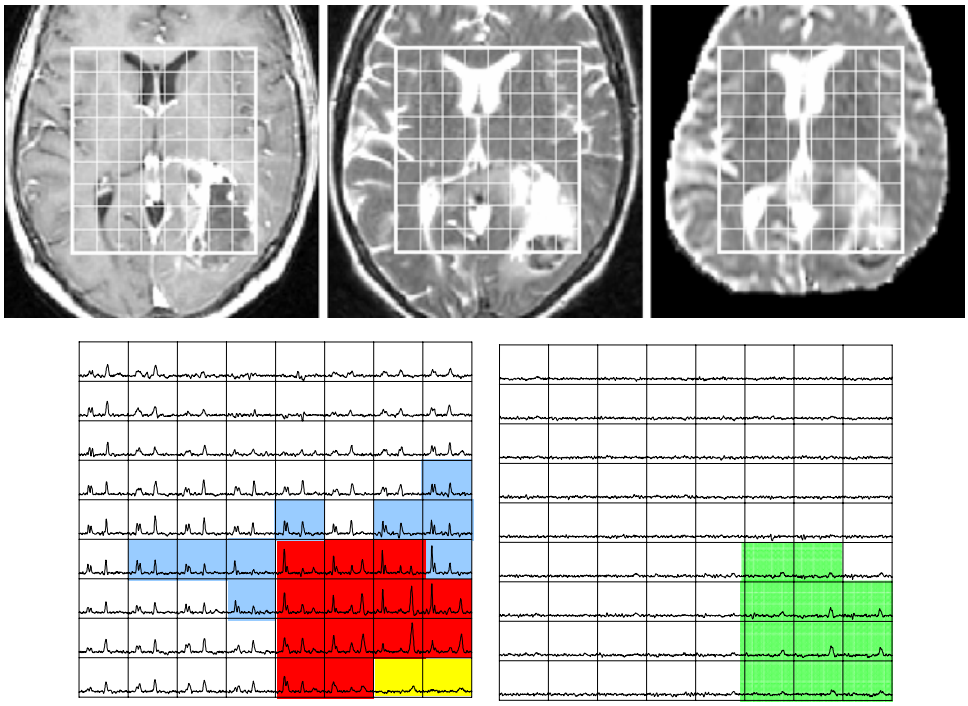

Fig. 8 MR images and spectra from a patient (G) who had a GBM with a moderate T2 volume, relatively larger proportion of the lesion that was enhancing or necrotic and large number of voxels with elevated CNI and lipid. For this patient age = 59, survival 104 days, voxels with CNI > 2 = 80, number of voxels with elevated lip = 45, sum of lipid intensities in CNI > 2 = 54.5, 10th percentile of nADC in the CEL = 0.91, %CEL + NEC = 66, T2ALL volume = 50 cc

2, sLAC(CNI > 2) and the sum of lipid peaks in the region with CNI greater than 2, sLIP(CNI > 2). Table 6 provides *P* values for these combinations. The combination of variables that gave the lowest *P* value of 0.0001 was sLIP(CNI > 2) and nADC10%(CEL). The examples in Figs. 6, 7 and 8 demonstrate how these values are expressed in patients who have long, medium and short survival, respectively. Note that the %(CEL + NEC) provided either no or minor improvements in *P* value when combined with the other variables.

Discussion

Perfusion, diffusion, and MR spectroscopic imaging are increasingly being used in clinical studies of patients with

Table 6 Proportional Hazards analysis of pairs of variables compared with the *P* values from the tests on individual variables

	sLIP(CNI2)	sLAC(CNI2)	nADC10%(CEL)	%CEL + NEC	v(nADC < 1.5)	v(CNI2)
Alone	0.003	0.038	0.028	0.026	0.047	0.044
v(CNI2)	0.006	0.058	0.076	0.019	0.100	
v(nADC < 1.5)	0.0004	0.034	0.023	0.049		
%CEL + NEC	0.005	0.022	0.023			
nADC10%(CEL)	0.0001	0.018				
sLAC(CNI2)	0.006					

Combinations that give the smallest *P* value are the ones that integrate the lipid and ADC parameters

GBM. It is therefore critical to determine how the data that they produce relates to anatomic images and whether the information provided can contribute to patient care. Although the current study considers parameters derived from imaging data that were obtained prior to surgery, it also provides information that is valuable in defining the questions that need to be addressed at other times during the course of the disease.

Information from the anatomic images

Key features observed in post-contrast T1-weighted MR images of brain tumors are the enhancing volume, which is assumed to represent the most malignant portion of the lesion, and the regions with hypointensity, which are assumed to correspond to necrosis. The corresponding T2-weighted images have regions of hyperintensity that are much larger then the enhancing and necrotic volumes and are assumed to include additional regions of infiltrative tumor and edema. None of the absolute volumes of these anatomic lesions on the pre-surgery images were predictive of outcome for this study. There are two possible explanations for this finding. Firstly, the highly variable and in some cases relatively large amount of edema present in the T2 hyperintensity may be a confounding factor. Evidence to support this comes from the relatively high values of ADC and low levels of the choline to NAA index within portions of the T2 hyperintensity. Secondly, it is important to realize that substantial portions of the enhancing and necrotic regions are typically removed during the subsequent surgery, which will affect the amount of residual disease and may influence the rate of recurrence [3–6]. While the extent of tissue resection that can be removed depends upon the location of the lesion within the brain, there were several patients in this study who had relatively large pre-surgery anatomic volumes who were assessed as receiving gross total resections and had longer survival that might have originally been anticipated. The observation that lesions with large percentages of the volume of T2 hyperintensity comprising either contrast enhancement or necrosis are likely to have worse survival may indicate that these characteristics are indicative of a more malignant phenotype as opposed to being a direct measure of tumor burden. This is a parameter that could readily be assessed in a semi-quantitative manner by the radiologist who is reading the images.

Information provided by the PWI data

The hemodynamic properties that were observed using perfusion-weighted imaging are consistent with published values for GBMs [41–43]. The median percentage of signal recovery for the ΔR2* curves in this pre-surgery population was 83% in the lesion compared with the baseline of 88% in NAWM. Although there was considerable heterogeneity within the lesion, these values are relatively modest compared with those observed in metastases or other types of lesions [44]. This implies that the blood brain barrier is still at least partially intact within regions of the enhancing volume. Poor delivery of therapeutic agents to the tumor is thought to be one reason why standard chemotherapy is only modestly successful for patients with GBM. As these treatments are typically given after surgical resection and during or after radiation, future studies should examine the impact that these have interventions have upon recovery values.

The presence of regions with increased microvascular density is a defining characteristic of malignant glioma [42]. Both the nCBV and ΔR2* peak height parameters have been proposed as surrogate measures of abnormal vascularity [43]. The nCBV intensities in our study were obtained by fitting the dynamic time curves with a gamma variate function that included a correction for vascular leakage [31, 33]. Peak heights were estimated using a simple non-parametric procedure [43]. The two sets of parameters were highly correlated and gave very similar results, implying that the information they contain is essentially equivalent. Although the most extreme values of nCBV and peak height were in the contrast enhancing regions, there were also sub-regions within the surrounding non-enhancing components of the lesion that were higher than normal appearing white matter. This is consistent with there being increased angiogenesis in portions of both the enhancing and non-enhancing lesion.

With the technology available during the acquisition phase of this study, the coverage for the perfusion images was limited to eight slices of about 3–6 mm each. This meant that only a portion of the tumor was studied for some of the larger lesions. Although the region from which data were acquired was chosen to be in the region that the radiologist felt would be most likely to have elevated perfusion, this incomplete coverage may have been a factor that limited the ability to use the estimated parameter in predicting outcome for these tumors. Now that MR scanners and multi-channel radiofrequency coils are routinely available in a clinical setting, the signal to noise ratio, coverage of the lesion and quality of the data can be significantly improved [45].

Information provided by the DWI data

There has been considerable variability in the values of ADC reported within tumors [46, 47]. The necrotic core of the tumor shows high ADC, indicating that necrosis may have destroyed the structural properties of the tissue, allowing water to more freely diffuse [48–50]. The T2-hyperintense region is higher in ADC than NAWM because of both vasogenic edema and the disruption of normal tissue structure. Although some of the diffusion weighted images had spatial distortions in regions close to the sinuses, the rigid registration was able to provide reasonable correlations within the regions of interest corresponding to the tumor. As with perfusion-weighted images, the availability of more advanced scanner hardware should be able to reduce the distortion and improve data quality for future studies.

The 10th percentile of ADC in the enhancing volume was significantly correlated with survival. This is consistent with observations from previous studies which have suggested that the presence of regions in GBM that have relatively lower ADC values indicates a higher density of tumor cells [13, 18, 51]. The volume of the region within the T2 hyperintensity with ADC less than 1.5 times the value in normal appearing white matter may be considered as a mechanism for distinguishing between infiltrative tumor and necrosis or edema. While this may adequately explain the behavior of these untreated tumors, the situation may be more complex in recurrent GBM or other gliomas, where the relationship between ADC and tumor cell density is unclear [13, 17, 18, 50, 51]. These results are particularly encouraging, because the capability for acquiring DWI data is widely available on state of the art clinical MR scanners and adds only a few minutes to the length of a standard examination. With a small investment in development of post-processing software it would be possible to routinely generate the parameters that have been identified as being predictive of survival.

Information provided by the MRSI data

The spectroscopic data provide parameters that reflect a number of different aspects of cellular metabolism [9, 11, 12, 22, 38]. Choline is a marker of cell proliferation and increased membrane turnover. This was increased within both enhancing and non-enhancing regions of GBMs. NAA is present in healthy neuronal cell bodies and was decreased in all tumor regions, with the lowest value in necrosis. The choline to NAA index (CNI) is more sensitive than the measurements of levels of the individual metabolites [11, 40] and was seen to be elevated in all tumor regions. The number of voxels with elevated CNI was larger than the number of voxels corresponding to the enhancing volume, suggesting that this parameter can detect tumor infiltration into non-enhancing portions of the lesion. As proposed in previous studies, this may be helpful in defining regions that should be subjected to focal therapy and in defining tumor burden [9, 12, 22].

Lactate is a byproduct of anaerobic glycolysis, and its presence may indicate hypoxic tumor metabolism, tumor infiltration, and growth. Lipid has been associated with cellular breakdown and necrosis. These parameters were seen to be elevated in tumor relative to NAWM, with the highest values in voxels that were either within or adjacent to necrosis. The strong association between the sum of levels of lipid in voxels with CNI > 2 and survival suggests that the presence of regions that include both high tumor cell density and necrosis may be used as a marker of aggressive tumor. Because of the limited spatial resolution of the MRSI data it is not clear whether these regions are truly coincident or merely adjacent to each other. The most effective pairwise combination of variables in the proportional hazards analysis was an ADC marker that reflects high cell density in the enhancing volume combined with the sum of levels of lipid within the region with CNI > 2. This may support the conclusion that increased lipid and high cell density are indicative of malignant behavior.

Of interest is that, despite its relatively coarse spatial resolution, the MRSI data provided parameters exhibiting a relationship with survival that had the lowest P value. One explanation for this may be that this methodology gives information about the spatial distribution and levels of multiple metabolites, which are able to describe more complex features of the lesion than the individual intensity parameters. The parameter which appeared to be of the most interest for predicting survival was the sum of lipid peak intensities within the region having choline to NAA index greater than 2. This not only considers the levels of three different metabolites to classify within voxels from the tumor, but also utilizes the intensities of metabolite levels from voxels within white matter from the same patient to evaluate the deviation of the observed values from normal.

The acquisition time for the 3D MRSI data used this study was 19 min, which required a significant extension of the clinical MR examination. Our research group has recently shown that the data with similar signal to noise and spatial resolution can be obtained in less than 5 min using more sensitive multi-channel radiofrequency coils in conjunction with alternative k-space sampling or parallel reconstruction techniques and using a 3T MR scanner [52, 53]. An alternative strategy to shortening the acquisition time would be to reduce the spatial resolution. This is likely to be valuable for the analysis of smaller tumors and for more accurately defining tumor margins in order to target focal therapy. In either case it appears that the MRSI data provide new information that could make a major contribution to the management of patients with GBM.

Another limitation of the MRSI acquisition method used in this study was that it focused on obtaining data from a 3D rectangular region within the brain. This meant that some regions of the tumor were not covered. It is possible that such incomplete coverage could have led to an underestimate of the spatial extent of the metabolic lesion and future technical development should focus on methods that are able to increase coverage. Differences in spatial resolution between the anatomic and metabolic images may also have produced metabolite values in regions of necrosis that were higher than anticipated and that were less extreme metabolite levels in non-enhancing tumor. The increased sensitivity associated with the use of scanners with higher field strength may therefore be important for future investigations of this technology [52].

Conclusions

Patients with GBM are subjected to resection, chemotherapy and radiation therapy following their pre-surgery MRI examination. Information regarding the extent of resection and response to therapy are thought to be important for prediction of long-term outcome. This study has implicated quantitative parameters derived from diffusion weighted images and MR spectroscopic imaging data that are acquired prior to surgical resection as being predictive of survival. These measures of tumor burden were associated with worse outcome, regardless of the subsequent treatment. It is extremely important to identify patients with a poor prognosis before beginning trials of new therapies, as it may be possible that they would benefit from alternative therapeutic strategies. Other areas where anatomic imaging can provide ambiguous results and where the quantitative parameters considered in this study may be important are in characterizing response to treatments that include anti-angiogenic and anti-proliferative agents. Future studies should also consider the validation of non-invasive imaging based upon histological and molecular analysis of tissues obtained using image-guided surgery.

Acknowledgements This study was supported by UC Discovery grants LSIT01-10107 and ITL-BIO04-10148 funded in conjunction with GE Healthcare, and NIH grants R01 CA059880 and P50 CA97257.

References

1. Oh J, Henry RG, Pirzkall A, Lu Y, Li X, Catalaa I et al (2004) Survival analysis in patients with glioblastoma multiforme: predictive value of choline-to-N-acetylaspartate index, apparent diffusion coefficient, and relative cerebral blood volume. J Magn Reson Imaging 19:546–554. doi:10.1002/jmri.20039
2. Salvati M, Cervoni L, Artico M, Caruso R, Gagliardi FM (1998) Long-term survival in patients with supratentorial glioblastoma. J Neurooncol 36:61–64. doi:10.1023/A:1017926603341
3. Simpson JR, Horton J, Scott C, Curran WJ, Rubin P, Fischbach J et al (1993) Influence of location and extent of surgical resection on survival of patients with glioblastoma multiforme: results of three consecutive Radiation Therapy Oncology Group (RTOG) clinical trials. Int J Radiat Oncol Biol Phys 26:239–244
4. Kowalczuk A, Macdonald RL, Amidei C, Dohrmann G 3rd, Erickson RK, Hekmatpanah J et al (1997) Quantitative imaging study of extent of surgical resection and prognosis of malignant astrocytomas. Neurosurgery 41:1028–1036. doi:10.1097/00006123-199711000-00004 (discussion 1036–1038)
5. Lacroix M, Abi-Said D, Fourney DR, Gokaslan ZL, Shi W, De Monte F et al (2001) A multivariate analysis of 416 patients with glioblastoma multiforme: prognosis, extent of resection, and survival. J Neurosurg 95:190–198
6. Lamborn KR, Chang SM, Prados MD (2004) Prognostic factors for survival of patients with glioblastoma: recursive partitioning analysis. Neuro-Oncology 6:227–235. doi:10.1215/S1152851703000620
7. McLendon RE, Halperin EC (2003) Is the long-term survival of patients with intracranial glioblastoma multiforme overstated? Cancer 98:1745–1748. doi:10.1002/cncr.11666
8. Croteau D, Mikkelsen T (2001) Adults with newly diagnosed high-grade gliomas. Curr Treat Options Oncol 2:507–515. doi:10.1007/s11864-001-0072-y
9. Pirzkall A, McKnight TR, Graves EE, Carol MP, Sneed PK, Wara WW et al (2001) MR-spectroscopy guided target delineation for high-grade gliomas. Int J Radiat Oncol Biol Phys 50:915–928. doi:10.1016/S0360-3016(01)01548-6
10. Giese A, Westphal M (2001) Treatment of malignant glioma: a problem beyond the margins of resection. J Cancer Res Clin Oncol 127:217–225. doi:10.1007/s004320000188
11. McKnight TR, von dem Bussche MH, Vigneron DB, Lu Y, Berger MS, McDermott MW et al (2002) Histopathological validation of a three-dimensional magnetic resonance spectroscopy index as a predictor of tumor presence. J Neurosurg 97:794–802
12. Pirzkall A, Li X, Oh J, Chang S, Berger MS, Larson DA et al (2004) 3D MRSI for resected high-grade gliomas before RT: tumor extent according to metabolic activity in relation to MRI. Int J Radiat Oncol Biol Phys 59:126–137. doi:10.1016/j.ijrobp.2003.08.023
13. Chen J, Xia J, Zhou YC, Xia LM, Zhu WZ, Zou ML et al (2005) Correlation between magnetic resonance diffusion weighted imaging and cell density in astrocytoma. Zhonghua Zhong Liu Za Zhi 27:309–311

14. Fuss M, Wenz F, Essig M, Muenter M, Debus J, Herman TS et al (2001) Tumor angiogenesis of low-grade astrocytomas measured by dynamic susceptibility contrast-enhanced MRI (DSC-MRI) is predictive of local tumor control after radiation therapy. Int J Radiat Oncol Biol Phys 51:478–482. doi:10.1016/S0360-3016(01)01691-1
15. Rosen BR, Belliveau JW, Vevea JM, Brady TJ (1990) Perfusion imaging with NMR contrast agents. Magn Reson Med 14:249–265. doi:10.1002/mrm.1910140211
16. Chenevert TL, Stegman LD, Taylor JM, Robertson PL, Greenberg HS, Rehemtulla A et al (2000) Diffusion magnetic resonance imaging: an early surrogate marker of therapeutic efficacy in brain tumors. J Natl Cancer Inst 92:2029–2036. doi:10.1093/jnci/92.24.2029
17. Kono K, Inoue Y, Nakayama K, Shakudo M, Morino M, Ohata K et al (2001) The role of diffusion-weighted imaging in patients with brain tumors. AJNR Am J Neuroradiol 22:1081–1088
18. Sugahara T, Korogi Y, Kochi M, Ikushima I, Shigematu Y, Hirai T et al (1999) Usefulness of diffusion-weighted MRI with echo-planar technique in the evaluation of cellularity in gliomas. J Magn Reson Imaging 9:53–60. doi:10.1002/(SICI)1522-2586(199901)9:1<53::AID-JMRI7>3.0.CO;2-2
19. Mardor Y, Pfeffer R, Spiegelmann R, Roth Y, Maier SE, Nissim O et al (2003) Early detection of response to radiation therapy in patients with brain malignancies using conventional and high b-value diffusion-weighted magnetic resonance imaging. J Clin Oncol 21:1094–1100. doi:10.1200/JCO.2003.05.069
20. Kuznetsov YE, Caramanos Z, Antel SB, Preul MC, Leblanc R, Villemure JG et al (2003) Proton magnetic resonance spectroscopic imaging can predict length of survival in patients with supratentorial gliomas. Neurosurgery 53:565–574. doi:10.1227/01.NEU.0000079331.21178.8E (discussion 574–576)
21. Tarnawski R, Sokol M, Pieniazek P, Maciejewski B, Walecki J, Miszczyk L et al (2002) 1H-MRS in vivo predicts the early treatment outcome of postoperative radiotherapy for malignant gliomas. Int J Radiat Oncol Biol Phys 52:1271–1276. doi:10.1016/S0360-3016(01)02769-9
22. Li X, Jin H, Lu Y, Oh J, Chang S, Nelson SJ (2004) Identification of MRI and 1H MRSI parameters that may predict survival for patients with malignant gliomas. NMR Biomed 17:10–20. doi:10.1002/nbm.858
23. Barker FG 2nd, Prados MD, Chang SM, Gutin PH, Lamborn KR, Larson DA et al (1996) Radiation response and survival time in patients with glioblastoma multiforme. J Neurosurg 84:442–448
24. Gamburg ES, Regine WF, Patchell RA, Strottmann JM, Mohiuddin M, Young AB (2000) The prognostic significance of midline shift at presentation on survival in patients with glioblastoma multiforme. Int J Radiat Oncol Biol Phys 48:1359–1362. doi:10.1016/S0360-3016(00)01410-3
25. Keles GE, Lamborn KR, Chang SM, Prados MD, Berger MS (2004) Volume of residual disease as a predictor of outcome in adult patients with recurrent supratentorial glioblastomas multiforme who are undergoing chemotherapy. J Neurosurg 100:41–46
26. Kreth FW, Berlis A, Spiropoulou V, Faist M, Scheremet R, Rossner R et al (1999) The role of tumor resection in the treatment of glioblastoma multiforme in adults. Cancer 86:2117–2123. doi:10.1002/(SICI)1097-0142(19991115)86:10<2117::AID-CNCR33>3.0.CO;2-8
27. Keles GE, Anderson B, Berger MS (1999) The effect of extent of resection on time to tumor progression and survival in patients with glioblastoma multiforme of the cerebral hemisphere. Surg Neurol 52:371–379. doi:10.1016/S0090-3019(99)00103-2
28. Nelson SJ, Nalbandian AB, Proctor E, Vigneron DB (1994) Registration of images from sequential MR studies of the brain. J Magn Reson Imaging 4:877–883. doi:10.1002/jmri.1880040621
29. Saraswathy S (2006) Semi-automated segmentation of brain tumor lesions in MR images [abstract]. International Society of Magnetic Resonance Imaging, Seattle
30. Zhang Y, Brady M, Smith S (2001) Segmentation of brain MR images through a hidden Markov random field model and the expectation-maximization algorithm. IEEE Trans Med Imaging 20:45–57. doi:10.1109/42.906424
31. Chan AA, Nelson SJ (2004) Simplified gamma-variate fitting of perfusion curves. In: Biomedical imaging: macro to nano. IEEE international symposium, vol 2, pp 1067–1070
32. Johnson G, Wetzel SG, Cha S, Babb J, Tofts PS (2004) Measuring blood volume and vascular transfer constant from dynamic, T(2)*-weighted contrast-enhanced MRI. Magn Reson Med 51:961–968. doi:10.1002/mrm.20049
33. Lee MC, Cha S, Chang SM, Nelson SJ (2005) Dynamic susceptibility contrast perfusion imaging of radiation effects in normal-appearing brain tissue: changes in the first-pass and recirculation phases. J Magn Reson Imaging 21:683–693. doi:10.1002/jmri.20298
34. Hartkens T, Rueckert D, Schnabel JA, Hawkes DJ, Hill DLG (2002) VTK CISG registration toolkit: an open source software package for affine and non-rigid registration of single- and multimodal 3D images. [abstract] BVM 2002. Springer-Verlag, Leipzig
35. Moonen CT, von Kienlin M, van Zijl PC, Cohen J, Gillen J, Daly P et al (1989) Comparison of single-shot localization methods (STEAM and PRESS) for in vivo proton NMR spectroscopy. NMR Biomed 2:201–208. doi:10.1002/nbm.1940020506
36. Tran TK, Vigneron DB, Sailasuta N, Tropp J, Le Roux P, Kurhanewicz J et al (2000) Very selective suppression pulses for clinical MRSI studies of brain and prostate cancer. Magn Reson Med 43:23–33. doi:10.1002/(SICI)1522-2594(200001)43:1<23::AID-MRM4>3.0.CO;2-E
37. Star-Lack J, Spielman D, Adalsteinsson E, Kurhanewicz J, Terris DJ, Vigneron DB (1998) In vivo lactate editing with simultaneous detection of choline, creatine, NAA, and lipid singlets at 1.5 T using PRESS excitation with applications to the study of brain and head and neck tumors. J Magn Reson 133:243–254. doi:10.1006/jmre.1998.1458
38. Nelson SJ (2001) Analysis of volume MRI and MR spectroscopic imaging data for the evaluation of patients with brain tumors. Magn Reson Med 46:228–239. doi:10.1002/mrm.1183
39. Nelson SJ, Cha S (2003) Imaging glioblastoma multiforme. Cancer J 9:134–145. doi:10.1097/00130404-200303000-00009
40. McKnight TR, Noworolski SM, Vigneron DB, Nelson SJ (2001) An automated technique for the quantitative assessment of 3D-MRSI data from patients with glioma. J Magn Reson Imaging 13:167–177. doi:10.1002/1522-2586(200102)13:2<167::AID-JMRI1026>3.0.CO;2-K
41. Catalaa I, Henry R, Dillon WP, Graves EE, McKnight TR, Lu Y et al (2006) Perfusion, diffusion and spectroscopy values in newly diagnosed cerebral gliomas. NMR Biomed 19:463–475. doi:10.1002/nbm.1059
42. Law M, Yang S, Wang H, Babb JS, Johnson G, Cha S et al (2003) Glioma grading: sensitivity, specificity, and predictive values of perfusion MR imaging and proton MR spectroscopic imaging compared with conventional MR imaging. AJNR Am J Neuroradiol 24:1989–1998
43. Lupo JM, Cha S, Chang SM, Nelson SJ (2005) Dynamic susceptibility-weighted perfusion imaging of high-grade gliomas: characterization of spatial heterogeneity. AJNR Am J Neuroradiol 26:1446–1454
44. Cha S, Lupo JM, Chen MH, Lamborn KR, McDermott MW, Berger MS et al (2007) Differentiation of glioblastoma multiforme and single brain metastasis by peak height and percentage of signal intensity recovery derived from dynamic susceptibility-

weighted contrast-enhanced perfusion MR imaging. AJNR Am J Neuroradiol 28:1078–1084. doi:10.3174/ajnr.A0484
45. Lupo JM, Lee MC, Han ET, Cha S, Chang SM, Berger MS et al (2006) Feasibility of dynamic susceptibility contrast perfusion MR imaging at 3T using a standard quadrature head coil and eight-channel phased-array coil with and without SENSE reconstruction. J Magn Reson Imaging 24:520–529. doi:10.1002/jmri.20673
46. Rana AK, Wardlaw JM, Armitage PA, Bastin ME (2003) Apparent diffusion coefficient (ADC) measurements may be more reliable and reproducible than lesion volume on diffusion-weighted images from patients with acute ischaemic stroke-implications for study design. Magn Reson Imaging 21:617–624. doi:10.1016/S0730-725X(03)00087-0
47. Sinha S, Bastin ME, Whittle IR, Wardlaw JM (2002) Diffusion tensor MR imaging of high-grade cerebral gliomas. AJNR Am J Neuroradiol 23:520–527
48. Henkelman RM (1990) Diffusion-weighted MR imaging: a useful adjunct to clinical diagnosis or a scientific curiosity? AJNR Am J Neuroradiol 11:932–934
49. Le Bihan D, Douek P, Argyropoulou M, Turner R, Patronas N, Fulham M (1993) Diffusion and perfusion magnetic resonance imaging in brain tumors. Top Magn Reson Imaging 5:25–31. doi:10.1097/00002142-199300520-00005
50. Tien RD, Felsberg GJ, Friedman H, Brown M, MacFall J (1994) MR imaging of high-grade cerebral gliomas: value of diffusion-weighted echoplanar pulse sequences. AJR Am J Roentgenol 162:671–677
51. Gauvain KM, McKinstry RC, Mukherjee P, Perry A, Neil JJ, Kaufman BA et al (2001) Evaluating pediatric brain tumor cellularity with diffusion-tensor imaging. AJR Am J Roentgenol 177:449–454
52. Li Y, Osorio JA, Ozturk-Isik E, Chen AP, Xu D, Crane JC et al (2006) Considerations in applying 3D PRESS H-1 brain MRSI with an eight-channel phased-array coil at 3 T. Magn Reson Imaging 24:1295–1302. doi:10.1016/j.mri.2006.07.012
53. Ozturk E, Banerjee S, Majumdar S, Nelson SJ (2006) Partially parallel MR spectroscopic imaging of gliomas at 3T. Conf Proc IEEE Eng Med Biol Soc 1:493–496